An internet of things-based intensity and time-resolved fluorescence reader for point-of-care testing

Authors & affiliations: O. Alonso[1], N. Franch[1], J. Canals[1], K. Arias-Alpízar[2], E. de la Serna[2], E. Baldrich[2,3], A. Diéguez[1]

[1]*Department of Electronics and Biomedical Engineering, University of Barcelona, Carrer Marti i Franques. 1, 08028 Barcelona, Spain.*

[2]*Diagnostic Nanotools Group, Molecular Biology and Biochemistry Research Center for Nanomedicine (CIBBIM-Nanomedicine). Vall d'Hebron Hospital Research Institute (VHIR). Passeig Vall d'Hebron 119-129; 08035 Barcelona, Spain.*

[3]CIBER de Bioingeniería, Biomateriales y Nanomedicina (CIBER-BBN), Spain

Abstract

A miniature internet of things (IoT)-based point-of-care testing (PoCT) fluorescence reader, able to perform both intensity and time-resolved measurements of different fluorescent tags, is presented. This low cost platform has been conceived for performing tests in low-resource and remote settings, displaying versatile performance and yet simple operation. It consists on an external case of 43x30x42 mm^3 (built in a 3D-printer) where all the elements are fixed, including some basic optics (3 lenses and 2 filters), a laser diode and a custom designed Single-Photon Avalanche Diodes (SPADs) camera. Both, the laser and the camera are controlled by a Field Programmable Gate Array (FPGA) with IoT capabilities.

The PoCT was validated by detecting *Plasmodium* antigen in a fluorescent enzyme-linked immunosorbent assay (ELISA) using a fluorescence substrate. The results were compared to those provided in parallel by two commercial fluorescent plate readers. As it will be shown, the PoCT fluorescent readout was more sensitive than its colorimetric counterpart. Furthermore, the PoCT displayed similar signal trends and levels of detection than the bulkier and more expensive commercial fluorescence plate readers. These results demonstrate that the PoCT platform developed could bring the performance of central laboratory assay techniques closer to the end-user level.

Keywords: Rapid diagnostic test (RDT); single board computer (SBC); miniature fluorescent microscope; decay time; SPADs detector; malaria diagnosis

1. Introduction

Population is ageing, which increases the numbers of elderly patients who require healthcare for age-sensitive conditions. The World Health Organization (WHO) reported that those numbers will continue to rise for many years to come. As an example, between 2015 and 2050 the proportion of the world's population over 60 years will nearly double from 12% to 22% (WHO, 2015). In rural settings or low- and middle-income countries, scarcity of resources, population growth, low levels of education and poor infrastructures make difficult to access to the health system (Clifford, 2016). One of the consequences of poor access to healthcare services is the delay in the diagnosis of diseases, which can be crucial to save the life of the patients and to avoid the spreading of infectious diseases (Boniface et al., 2012; Mashamba-Thompson et al., 2018; Sharma et al., 2015).

The WHO is calling for new tools and clinical methods that could operate in settings with limited access to laboratory services (Mabey et al., 2004). In this scenario, point-of-care testing (PoCT)

takes special relevance since it brings the clinical laboratory close to the patient for early diagnosis. The main benefits of PoCT are the portability, ease of use and rapid turnaround time for results, which provides disease diagnosis, monitoring, and management close to the patient, and allows to establish a personalized therapy, improving the life of the patients and reducing the global costs for the National Health Systems (Vashist, 2017). However, for this to happen, it must be demonstrated that the results provided by the PoCT device are accurate compared to core laboratory testing and thus acceptable for diagnosis (Lightbody et al., 2017).

PoCT devices are useful in several applications such as diagnosis of infectious, immunological, cardiovascular, oncological, and neurodegenerative diseases, as well as in blood, genetic and microbiology testing, among others. In all these possible applications, the most common and most inexpensive method of imaging analysis is fluorescence (Cholkar et al., 2017; Pennathur and Fygenson, 2008). Different PoCT devices using fluorescence as the transduction method are reported in the literature (Boppart and Richards-Kortum, 2014; Fang et al., 2016; Obahiagbon et al., 2018; Pais et al., 2008; Ryu et al., 2011; Wang et al., 2017; Watkins et al., 2013; Wei et al., 2017). All these works show the efficiency and good performance of these types of tests, pointing to the need to improve the limit of detection (LOD) and miniaturize the reading devices.

Typically, fluorescent PoCT devices detect the presence of a certain substance by performing intensity measurements. In these assays, the sample is continuously illuminated by the excitation light. In the presence of the targeted analyte, the sample starts emitting fluorescent light. This emitting light is monitored and used to quantify a biochemical reaction or binding event, providing good accuracy, sensitivity (single molecule detection), and targeted labelling of biological samples (Léonard et al., 2014). The main drawback of these assays is their dependence on parameters such as fluorophore excitation wavelength and concentration, which can lead to misinterpretation of the obtained results. One solution to overcome the limitations of intensity assays is by using time-resolved techniques like Time-Correlated Single Photon Counting (TCSPC) (Canals et al., 2019; Dutton et al., 2015). In this measurement setup, the sample is illuminated by a short light pulse that causes the sample to start emitting fluorescent light. As the sample is not excited any more, it is possible to measure the fluorescence decay of the fluorophore. Because the decay time is an intrinsic molecular property, it is independent of fluorophore concentration and excitation intensity (Berezin and Achilefu, 2010). Furthermore, time-resolved fluorescence improves the specificity of the measurements by time domain discrimination, allowing to discern the light of interest from the background noise (Kobayashi et al., 2010) and permitting the differentiation of fluorophores with different lifetimes in multiplexed assays (Luo et al., 2018; Salthouse et al., 2008).

In this work, we present a miniature, internet of things (IoT)-based, general-purpose PoCT, which could overcome the limitations of current PoCT diagnostic systems and provide worldwide implementation, including in rural and low- and middle-income settings. The PoCT is based on the classical setup of a fluorescence microscope. The main element is a proprietary Single-Photon Avalanche Diodes (SPADs) camera, which is used as the sensing system. The SPADs camera, allows to perform fluorescence intensity assays as well as time-resolved measurements. Remote control of the PoCT device is possible through the enabled IoT capabilities and the results can be stored in the cloud, which would facilitate remote assay operation and/or interpretation. The performance of the PoCT device was assessed by detecting *Plasmodium* antigen (a biomarker of malaria infection) in an enzyme-linked immunosorbent assay (ELISA) using a fluorescent substrate. As it will be shown, the results were comparable to

those provided by two commercial ELISA fluorescence plate readers, demonstrating the high performance of the low-cost POCT platform produced.

This paper is structured as follows: in Section2, we describe the development of the instrument, entering in detail on the materials and techniques used to build our IoT-based PoCT. In Section 3, we present the experimental results, the initial tests performed to characterize the system and the application of our PoCT detecting *Plasmodium* antigen using a fluorescent ELISA substrate. The results and the costs of the PoCT are discussed by comparing them with two commercial ELISA plate readers. Finally, we conclude with a discussion showing the pros and cons of the IoT-based PoCT.

2. Materials and methods

Fluorescence-based PoCT devices are well documented in the literature (Fang et al., 2016; Obahiagbon et al., 2018; Ryu et al., 2011). The major contribution of the present work is that the PoCT reader produced can perform both fluorescence intensity and time-resolved measurements maintaining a low production cost. In addition, the laser diode, dichroic mirror and filters employed can be easily interchanged by similar components with different optical properties, allowing the PoCT to be easily tuned to perform tests with other excitation and emission wavelengths. Nevertheless, in this paper, only the optics necessary for the detection of recombinant lactate dehydrogenase from *Plasmodium falciparum* (Pf-LDH) are described.

A schematic diagram of the PoCT is shown in Fig. 1(A). The PoCT consists on an external case (built in a 3D-printer) where all the elements are fixed, including some basic optics (3 lenses and 2 filters), a laser diode and a custom designed SPADs camera. Both, the laser and the camera are controlled by a Single Board Computer (SBC) with IoT capabilities. The complete system is presented in Fig. 1(B).

2.1. Production of the external case

The external case (43x30x42 mm^3) was designed with a 3D CAD design software (SolidWorks) and produced using a 3D printer (BCN3D+; Fundació CIM, Barcelona, Spain) with a precision of 0.1 mm. This case was used to place all the elements of the designed fluorescence microscope. Therefore, special attention on the distances and focal lengths of the optical components were considered in order to excite the sample with the greatest number of photons and to detect the maximum number of photons emitted by the sample. It also includes three holes for the screws that regulate the horizontal position of the SPADs camera board and its depth. A series of rims on the top of the case facilitate the insertion of microcapillary tubes, lateral flow strips or microscope slides for sample evaluation. Additionally, the case can be closed with a lid, shown in Fig. 1(B), designed to reduce the noise coming from the ambient light.

2.2. Optics' assembly

A laser diode (OSRAM, Munich, GE, ref. PL_520_B1, λ_{ex} = 520 nm, optical power 50 mW) is used to illuminate the sample. The driving circuit of the laser is included in the same board and has two operation modes. In continuous mode, used in intensity measurements, the driver fixes the current that supplies the laser diode. In pulsed mode, used in time-resolved measurements, the driver emits short electrical pulses of 1.6 ns full width at half maximum (FWHM). More details about the pulsing circuit can be found in (Canals et al., 2019).

As the laser diode is not collimated, some optics need to be included into the case (Fig.1(A)). For the excitation of the sample, the laser diode is placed in the focus of a first lens (Thorlabs, Munich, GE, ref. 220TM). At this point, all the light rays from the laser diode are parallel and are sent to the 45° dichroic mirror (PixelTeq, Largo, FL, USA, ref. 102291649). Fig. 1(C) shows the transmission/reflection bands of the 5 mm x 5 mm dichroic mirror. The λ_{ex} = 520 nm wavelength is completely reflected into the mirror and the light rays are sent towards the sample. A second lens (Thorlabs, Munich, GE, ref. 110TM), placed between the dichroic mirror and the sample, sends the parallel light rays to the focus of the lens, where the sample will be placed. The dichroic mirror will transmit those parallel rays down to the SPADs camera across two more optical elements. Near to the dichroic, a 5 mm x 5mm band pass filter (PixelTeq, Largo, FL, USA, ref. CO674-71, λ_{em} = 600nm, FWHM 13nm) is used to filter out the entire excitation range of the fluorophore and to transmit the emission light of that fluorophore (Fig. 1(C)). Before the SPADs camera, another 110TM lens focuses all the parallel rays over the SPADs camera. The dichroic mirror and the band pass filter were selected to be used in experiments in which the fluorescence emission is redshifted from the excitation band.

2.3. Description of the SPADs camera

The SPADs camera was used to sense either fluorescence intensity or decay time with the aid of an external Time-to-Digital converter (TDC) implemented on a Field Programmable Gate Array (FPGA).

The SPADs array chip was fabricated in 0.35 µm HV-CMOS AMS technology, which granted lower noise than other production paths (Bronzi et al., 2016). The SPADs are biased above its breakdown voltage (i.e. Geiger mode) and operated in gated mode, which reduces the probability to detect noise (Vilella and Diéguez, 2012).

Fig. 1(D) shows a picture of the chip which is 2.93x1.98 mm^2, including a 1 x 1 mm^2 SPADs camera, with 1.6% fill factor. The camera is composed by an array of 16x16 round SPADs of 10 µm of diameter and pitch of 70 µm (marked light blue in Fig.1(D)) connected in rolling shutter mode for the readout and configuration. All the Input/Output (I/Os) pads used to control de camera are distributed on one side of the chip (right in the Fig. 1(C)). In this way, the SPADs array can be on the chip edge and the alignment of the sensing area with the focus of light is easier.

2.4. Single Board Computer (SBC)

The laser diode and the SPADs camera are controlled by a low-cost and high-performance SBC built around the Xilinx Zynq-7010 (XC7Z010). This is a Programmable System-on-Chip (SoC) that integrates a dual-core ARM Cortex-A9 processor with a Xilinx 7-series FPGA logic. The FPGA part of the SBC includes the digital control of the SPADs camera and the TDC. The TDC has a precision of 50 ps for the fluorescence decay time measurement. The ARM processors are used to run a Linux operating system, simplifying all the networking operations that can be performed via the 10/100/1000M Ethernet port or via a USB Wifi Dongle connected to the USB port, both included in the SBC. IoT capabilities can be activated since the SBC is connected to the Network. This PoCT enables IoT using a private platform named ThingSpeak™.

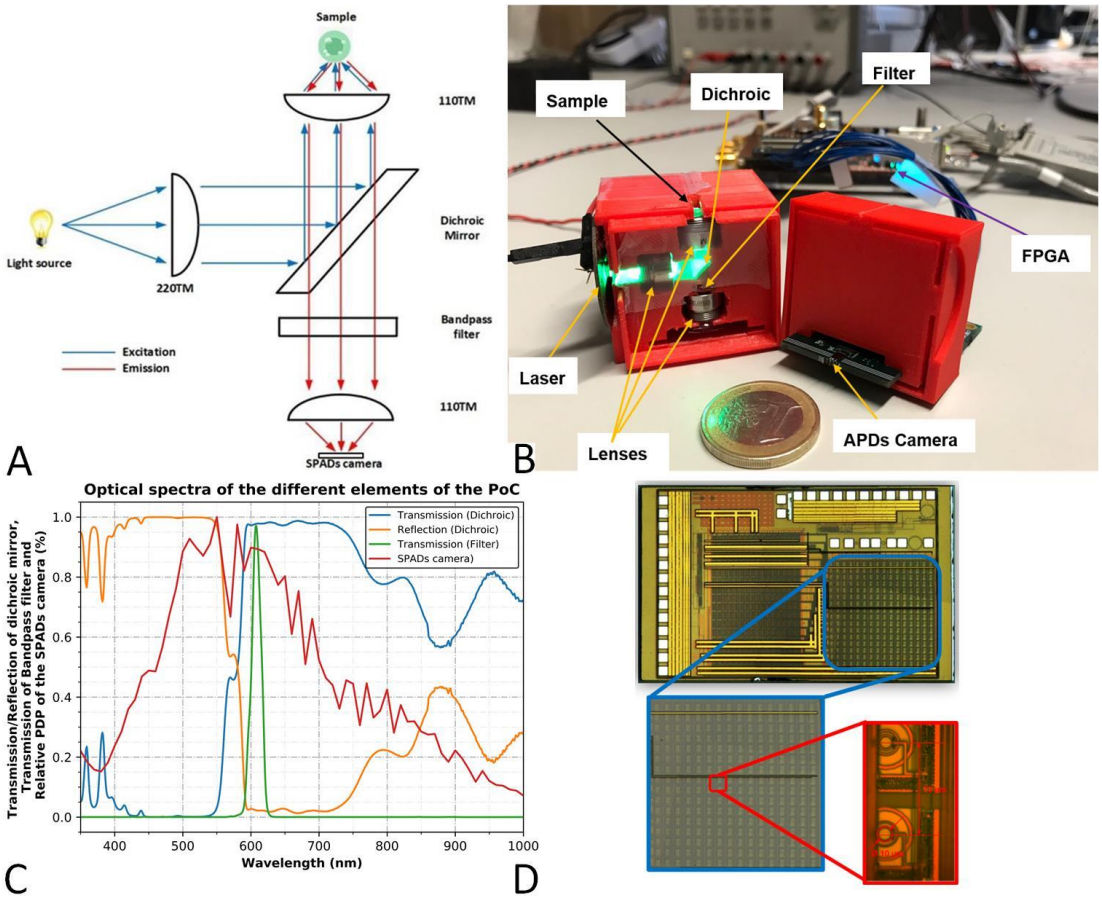

Fig. 1. (A) Schematic representation of the miniature fluorescent microscope including all the optical components and the sensor (SPADs camera). Blue lines indicate the path of the excitation light, red lines indicate the path of the emission light. (B) Picture of the complete miniature fluorescent microscope including the controlling board (FPGA). (C) Transmission and reflection spectra of the dichroic mirror (blue and orange lines respectively), transmission spectra of the band pass filter (green line) and the photon detection probability of the SPADs camera. (D) Picture of the chip fabricated in 0.35 µm HV-CMOS AMS technology. The SPADs array is marked in light blue, a zoom of the pixel with a SPAD of 10 µm is marked in red.

2.5. Pf-LDH detection by ELISA

Pf-LDH was provided by CTK Biotech (San Diego, USA). Anti-PLDH monoclonal capture and detection antibodies (c-Ab and d-Ab) were from BiosPacific (California, USA). Streptavidin Poly-HRP (Ref. 21140) and QuantaRed™ Enhanced Chemifluorescent HRP Substrate (Ref. 15159) were obtained from Thermo Fisher (Waltham, USA). Phosphate-buffered saline tablets (PBS; pH=7.4) were obtained from Gibco (Life Technologies, Madrid, Spain). Microtitter plates with 96-wells were purchased from Corning (Corning B.V. Life Sciences; Amsterdam, The Netherlands).

A sandwich ELISA assay was carried out using the pair of antibodies described before. Unless otherwise stated, incubations were performed with 100 µL of solution per well, for 1 h at 37°C, inside a thermostated incubator. Each incubation was followed by three consecutive washes with PBS, Tween 20 0.05% (PBS-T; 200 µL per well).

First, the microtiter plates were modified for 1 h with c-Ab (2.5 µg mL^{-1} in PBS). The plates were then blocked with BSA 1 % (PBS-BSA1%) for 1 h to prevent non-specific binding. Incubations followed with Pf-LDH and biotinylated d-Ab (0.016–100 ng mL^{-1} and 37.5 ng mL^{-1}, respectively,

in PBS-T with BSA 1%, PBS-T-BSA1%). Streptavidin-HRP was then added (1:200 in PBS-T-BSA1%) to the wells and was incubated at room temperature for 20 min. The fluorescence substrate (QuantaRed™ working solution) was then incubated at room temperature for 5 min, before stopping the reaction with QuantaRed™ stopping solution (10 µL per well) and measuring fluorescence. This substrate solution contained 10-acetyl3.7-dihydroxyphenoxazine (ADHP), which was hydrolyzed by the enzymatic HRP label into the highly fluorescent and soluble product resorufin.

3. Results and discussion

3.1. CMOS SPADs sensor characterization

The main parameters characterizing individual SPADs are noise and sensitivity. Noise, measured as the rate of spurious pulses due to thermal events or dark count rate (DCR), was variable due to its dependence on the number of traps in the diode. DCR was measured across the SPADs array for different chips, to determine its variability between devices. The DCR was below 1 KHz for 90% of the pixels. The absolute minimum noise for this overvoltage was found to be 300 Hz for this array design. On the other hand, sensitivity was measured as photon detection probability (PDP). The PDP was measured using an electro-optical bench composed by a white-light source, a monochromator filter and a calibrated reference detector. Fig. 1(C) shows the PDP of the SPADs in a wavelength range 300-1100 nm for overvoltages of 1.3 V and 1.8 V, at room temperature. The SPADs were mostly sensitive between wavelengths of 400 and 800 nm, but the PDP was always below 15%. This is due to the presence of a polyimide layer covering the chip in this technological process. Although the use of this layer can be avoided during chip production (Niclass et al., 2006), this would leave the chip unprotected.

The PoCT was characterized additionally using a commercial fluorescent label, Qdot™ 605 (ThermoFisher Scientific). This fluorescent label has emission maxima at ~605 nm and is excited with green light, although ultraviolet light excites the molecule more efficiently.

The laser diode is current-controlled, which means that it is possible to increase or decrease the light power. More photons from the laser diode reach the camera when the light power is increased. Therefore, the measured counts include counts from the excitation light as well as the emission light. For this reason, the first tests were conducted to find the Signal to Noise (S/N) ratio depending on the used light power. In other words, the number of counts measured in the presence of a fluorescent sample/tag compared to the counts measured in its absence. Fig. 2(A) shows the measured S/N ratio when different currents were supplied to the laser diode. For this test 1 µL of Qdot™ 605 (1 µM) was introduced in a microcapillary and measured by the PoCT. The camera used an observation window of 290 ns and repeated the operation until accumulating a total measurement time of 1 s, which took ~ 3 s. The best S/N ratio was obtained when supplying 60 mA. Therefore, this current was fixed for the subsequent tests.

Qdot™ 605 were next diluted serially in PBS (1, 1/2, 1/4, 1/8, 1/16, 1/32, 1/64, 1/128 µM and 1/256 µM). Fig. 2(B) shows the number of counts measured for each concentration, sensing 10,000 times with the SPADs camera and using different observation windows. PBS without Qdot™ 605 was also measured as the negative control, and to calculate the LOD (3σ) and the limit of quantification (LOQ; 10σ). LOQ is illustrated in Fig. 2(B) as a horizontal line for each observation window, meaning that all the measures above the LOQ line can be quantified. From Fig. 2(B), it can be concluded that the use of long observation windows (i.e. 10 µs) improves the detection at low concentrations, while short observation windows (i.e. 10 ns) must be used for high concentrations in order not to saturate the camera (Dutton et al., 2018).

In time-resolved mode, the laser diode is pulsed using the electronic circuit presented in (Canals et al., 2019). The laser is biased at 10 mA to obtain a higher optical pulse. The measurement of the decay time starts by opening an observation window of 400 ns. During this time, a short pulse is emitted by the diode laser. After that, if the sample contains Qdot™ 605, it starts emitting fluorescent light. The TDC discretizes the observation window in 8,000 sub-windows (50 ps each) and then measures the time of arrival of the first detected photon by the SPAD pixel, adding one count to the corresponding sub-window. This test is repeated approximately 500 million times. The acquisition time lasts ~7 minutes. The result is a histogram that follows the probability of distribution of the Qdot™ 605 emission. Fig. 2(C) shows the histogram obtained from Qdot™ 605 at a concentration 1/32 µM. The histogram of the measurement of PBS without Qdot™ 605 is also included to show the response of the laser diode pulse. In Fig. 2(C) the Y axis shows the natural logarithm of the received counts. Since the fluorescence decay is exponential, the decay time can be calculated using a linear regression in the area of interest, in which the decay time corresponds to the inverse of the slope of the resulting line. In this case, the area of interest is found after the laser diode pulse and is marked by two black vertical lines. A decay time of around 35 ns was calculated for Qdot™ 605 1/32 µM, which is in agreement with those in the literature (Gaigalas et al., 2014).

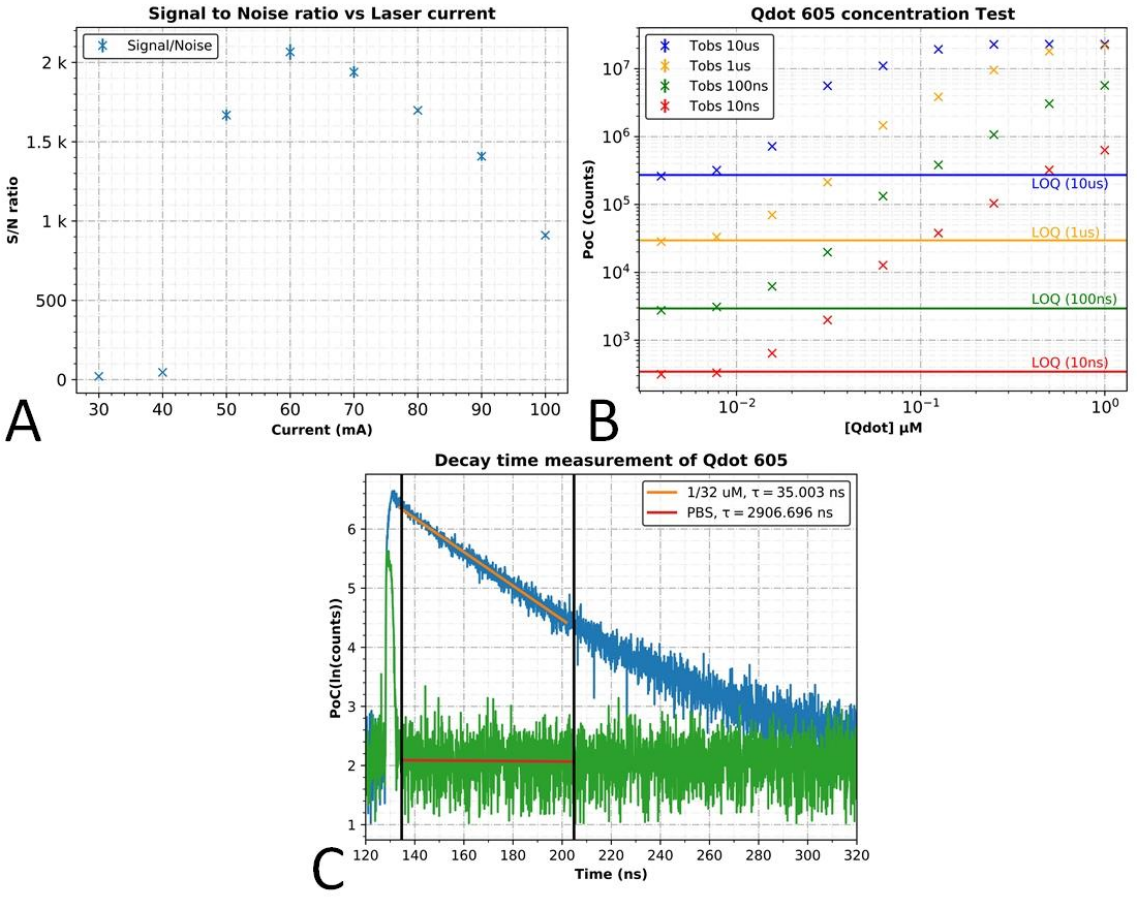

Fig. 2. (A) S/N ratio measured for a fixed concentration of Qdot™ 605 (1 µM) when the laser diode was supplied with increasing currents. (B) Total number of counts acquired in 10,000 measurements with the SPADs camera, using different Qdot™ 605 concentrations (1, 1/2, 1/4, 1/8, 1/16, 1/32, 1/64, 1/128 µM and 1/256 µM). The measurements have been done using 4 different observation windows (10 µs, 1 µs, 100 ns and 10 ns). The LOQ for each observation windows is represented as a horizontal line. (C) Decay time measurement of Qdot™ 605 (blue line), with a 1/32 µM concentration. The measurement of the pulse of the laser (green line) is also included.

3.2. PoCT application to malaria diagnosis

Malaria is a treatable infectious disease caused by *Plasmodium* spp. and transmitted by the bite of infected anopheles female mosquitos (Markwalter et al., 2016). According to the WHO, more than three billion people are at risk of acquiring malaria (WHO, 2018). Only in 2017, malaria produced 219 million cases of infection (92% in Africa) and 435,000 casualties, 61% of them among children aged under 5 years (WHO, 2017). Early diagnosis is the most effective strategy to prevent malaria complication into severe cases and patient dead. Among the biomarkers available for early malaria diagnosis, parasite LDH is present in all the *Plasmodium* species that infect humans (Markwalter et al., 2016). This contrasts with other biomarkers, such as histidine rich protein (HRPII), which is specific to *Plasmodium falciparum* (Brown et al., 2004).

Pf-LDH ELISA assay has demonstrated to be a valid tool to detect the parasite (Atchade et al., 2013; Kwenti et al., 2017). Therefore, a Pf-LDH sandwich ELISA was used to demonstrate the functionality of our miniature, IoT-based, general-purpose PoCT reader. Serial dilutions of Pf-LDH were analyzed in each experiment, including 11 concentrations spanning between 9.8 pg mL^{-1} and 100 ng mL^{-1}, plus the negative controls without Pf-LDH. As the PoCT is based on a fluorescence microscope, the Pf-LDH ELISA was detected using a peroxidase enzyme tag (HRP) and a fluorescent enzymatic substrate (QuantaRed™). In the presence of Pf-LDH, HRP bound to the plate and hydrolyzed QuantaRed™ into resorufin, which is fluorescent. For PoCT detection, samples were transferred to a microscope slide. The maximum absorption of resorufin occurs at an excitation wavelength λ_{ex} = 563 nm, and reached 50% absorption using the PoCT laser diode (λ_{ex} = 520 nm). Resorufin exhibits maximal emission at λ_{em} = 587 nm and a fluorescence lifetime close to 3 ns (Ryder et al., 2003).

In intensity measurements, the SPADs camera was aligned in order to obtain the maximum number of photons coming from the sample. The PoCT has been designed to have a 1:1 relation between the sample and the image created at the SPADs camera, therefore light is not magnified nor concentrated. As discussed in section 2.3, the SPADs camera has 1.6% fill factor, which means that a big proportion of light is lost when it is not concentrated into a single pixel. In order to minimize this drawback, all the pixels where the sample image was formed were considered jointly as if the SPADs camera was a silicon photomultiplier. In addition, each sample was measured 3 times using different observation windows (Tow = 126 ns, 290 ns and 400 ns) and each observation window was analyzed 2.5 million times, obtaining a total observation time of 0.315 s, 0.725 s and 1 s, respectively. After this, the counts of each test were summed up in order to increase the dynamic range of the SPADs camera, as reported in (Dutton et al., 2018). Basically, the sum method compensates for the effect of having samples that produce much more light than others. Short observation times are needed for high concentrations in order not to saturate the sensor. On the other hand, for low concentrations, long observation times can increase the number of photons detected. Finally, the Pf-LDH ELISA assay was repeated 4 times to increase the statistics.

Fig. 3(A) summarizes the counts obtained by the PoCT for different concentrations of Pf-LDH, after applying the sum method. The black line shows the counts measured for the negative control (616,618 counts, with a variance σ_{NC} = 8,355.3 counts). The purple and blue lines indicate the LOD (641,683.9counts) and LOQ (700,171 counts), respectively. With the sum method, all the measured Pf-LDH concentrations were above the LOQ. Without using the sum method, the measurements of the 5 lowest Pf-LDH concentrations tested were below or around the LOQ.

These results were compared with those obtained in parallel using two commercial fluorescent plate readers available at our facilities, the *Thermo Fisher Appliskan* (λex = 544 nm; λem = 590 nm) and the *Bio Tek FLx 800* (λex = 530 nm; λem = 590 nm), with prices ranging between 2,500 $ and 5,000 $ for a second-hand equipment. In general, and although the arbitrary fluorescence units displayed by each of them could not be directly compared, the three equipment produced similar signal trends. Nevertheless, the customized PoCT device displayed signal saturation at a lower analyte concentration and higher signal variability. This was attributed to the fact that, while the commercial equipment measured simultaneously all the wells of an ELISA plate, the PoCT measured samples one-by-one. In spite of this, the counts obtained by the PoCT correlated linearly with the counts measured by the commercial plate readers for each Pf-LDH concentration (Fig. 3(B)), which is a first indication that the PoCT is a valid instrument. This was confirmed by comparing the S/N provided by the 3 equipment for low Pf-LDH concentrations (Fig. 4(A)). If a S/N cut-off of 2 was established, the PoCT detected similar or lower concentrations than the two commercial instruments.

Finally, resorufin was also measured in the decay time mode. In this case, only one SPAD pixel was used. Figure 4(B) shows the results of the decay times measured for 3 different concentrations of Pf-LDH (100 ng/ml, 12.5 ng/ml and 9.8 pg/ml). As the laser diode was excited during the observation window, the result obtained with the negative control is also included to reflect the effect of the laser on the measurements. The decay times measured for each concentration were 2.85, 3.14 and 4.61 ns, respectively, which are close to the 3 ns reported previously (Ryder et al., 2003).

3.3. Advantages of the PoCT

The PoCT has been validated for malaria diagnosis because this disease has special incidence in low- and middle-income countries, where the use of a rapid test that can be controlled remotely may be crucial. The results obtained from several assays demonstrate that the measure of fluorescence intensity with the PoCT is comparable to that provided by commercial instruments, which were significantly bulkier and costlier. Unlike such commercial instruments, the PoCT can also measure fluorescence decay time with good accuracy.

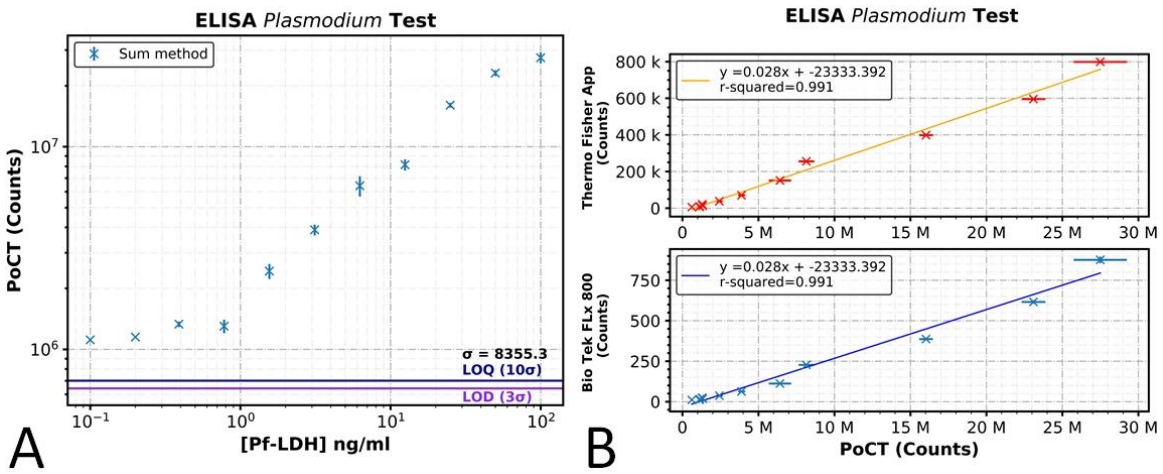

Fig. 3. (A) Counts obtained by the PoCT measuring different concentrations of Pf-LDH. The sum method, described in section 3.3, was applied in order to increase the dynamic range of the SPADs camera. LOD and LOQ are represented as horizontal lines. (B) Results obtained with the PoCT are compared with the results obtained using two commercial fluorescent plate readers. In both cases, the results correlate linearly.

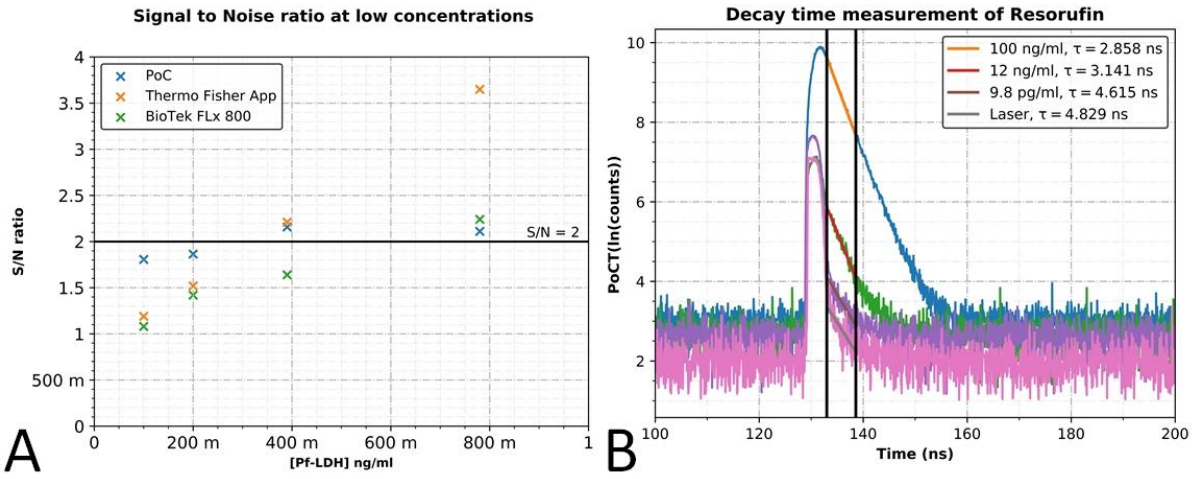

Fig. 4. (A) S/N ratio measured in each instrument for low Pf-LDH concentrations. (B) Lifetime measurements for different Pf-LDH concentrations (100 ng/ml, 12.5 ng/ml and 9.8 pg/ml). The pulse of the laser is also included.

The cost of the PoCT is summarized in Table 1. Even in the prototyping phase, where the cost of the products is higher than in the production phase, the total cost of the PoCT is much lower than commercial products.

Components	Cost	Cost per device	Notes
SPADs camera chip (40 chips fabricated in a multi-project wafer)	7000 €	175 €	1
FPGA board (MYS-7Z010)	76.05 €	76.05 €	
Laser driver circuit (includes all electronics parts and components)	96 €	96 €	
A220TM lens	81.89 €	81.89 €	
A110TM lens	152.96 €	76.48 €	
Bandpass filter, 600nm FWHM 13nm	65 $	65 $	2
45 Deg Dichroic Mirror Filter - Green	70 $	70 $	2
Fabrication of Printed Circuit Boards (PCBs)	360 €	30 €	1

1 the production of a larger volume of chips/PCBs dramatically reduces the cost

2 Price can be lowered more than 25% for orders with a larger volume of components

4. Conclusions

A miniature, IoT-based, general-purpose and highly sensitive fluorescence platform, capable of performing intensity and time-resolved measures, has been presented. Apart from the characterization with a commercial fluorescent label (Qdot™ 605), device performance was demonstrated by detecting *Plasmodium falciparum* in a fluorescent Pf-LDH ELISA assay. The PoCT reader showed the same precision than commercial and bulky instruments in intensity assays, and good accuracy in time-resolved assays compared with the literature. The total production cost of the device is approximately 750 €, which is economical compared to the price of most commercial instruments. The time spent in each measurement in the Pf-LDH ELISA assay is low. It only needs 3 seconds for an intensity measurement and 7 minutes for a time-resolved measurement, which confirms the device utility for rapid testing. Furthermore, the presented PoCT has IoT capabilities, which is compatible with remote control PoCT operation, using a cellphone, laptop or a computer, and with result storage in the cloud, which would allow any doctor in the world to access and review them.

Competing interests

The authors declare no competing financial interest.

Acknowledgements

This work was supported in part by ACC1Ó in Catalonia through the Project "Portable device for molecular diagnosis" coded VALTEC13-1-0020-00; AGAUR via the project 'Chip for Molecular Diagnosis' (2014LLAVOR00003); and by grants (i) CPII18/00025 and DTS17/00145 (co-funded by Fondo de Investigaciones Sanitarias of the Instituto de Salud Carlos III (ISCIII) and the European Regional Development Fund (ERDF). It also received support of two fellowships from "La Caixa" Foundation (ID 100010434 (KAA) and Caixaimpulse CI17-00037), and from the European Union´s Horizon 2020 research and innovation programme under the Marie Skłodowska Curie, grant agreement No. 713673, and under H2020 FET-OPEN project Chipscope, grant agreement No 737089. EdS is funded by a PERIS grant (SLT002/16/00316) from the Departament de Salut of the Generalitat de Catalunya (Spain). Diagnostic Nanotools is a Consolidated Group supported by the Secretaria d'Universitats i Recerca del Departament d'Empresa i Coneixement, Generalitat de Catalunya (Grant 2017 SGR 240).

References

Atchade, P.S., Doderer-Lang, C., Chabi, N., Perrotey, S., Abdelrahman, T., Akpovi, C.D., Anani, L., Bigot, A., Sanni, A., Candolfi, E., 2013. Malar. J. 12, 279–289.

Berezin, M.Y., Achilefu, S., 2010. Chem. Rev. 110, 2641–2684.

Boniface, R., Moshabela, M., Zulliger, R., MacPherson, P., Nyasulu, P., 2012. Tuberc. Res. Treat. 2012, 1–7.

Boppart, S.A., Richards-Kortum, R., 2014. Sci. Transl. Med. 6, 253–264.

Bronzi, D., Villa, F., Tisa, S., Tosi, A., Zappa, F., 2016. IEEE Sens. J. 16, 3–12.

Brown, W.M., Yowell, C.A., Hoard, A., Vander Jagt, T.A., Hunsaker, L.A., Deck, L.M., Royer, R.E., Piper, R.C., Dame, J.B., Makler, M.T., Vander Jagt, D.L., 2004. Biochemistry 43, 6219–6229.

Canals, J., Franch, N., Alonso, O., Vilà, A., Diéguez, A., 2019. Sensors. 19, 1–18.

Cholkar, K., Hirani, N.D., Natarajan, C., 2017, in: Emerging Nanotechnologies for Diagnostics, Drug Delivery and Medical Devices. Elsevier Inc., pp. 355–374.

Clifford, G.D., 2016. J. Med. Eng. Technol. 40, 336–341.

Dutton, N., Al Abbas, T., Gyongy, I., Mattioli Della Rocca, F., Henderson, R., 2018. Sensors 18, 1166–1178.

Dutton, N.A.W., Gnecchi, S., Parmesan, L., Holmes, A.J., Rae, B., Grant, L.A., Henderson, R.K., 2015. Proc. IEEE Int. Solid-State Circuits Conf. 204–206.

Fang, X.X., Li, H.Y., Fang, P., Pan, J.Z., Fang, Q., 2016. Talanta 150, 135–141.

Gaigalas, A.K., DeRose, P., Wang, L., Zhang, Y.-Z., 2014. J. Res. Natl. Inst. Stand. Technol. 119, 610–28.

Kobayashi, H., Ogawa, M., Alford, R., Choyke, P.L., Urano, Y., 2010. Chem. Rev. 110, 2620–2640.

Kwenti, T.E., Njunda, L.A., Tsamul, B., Nsagha, S.D., Assob, N.J.C., Tufon, K.A., Meriki, D.H., Orock, E.G., 2017. Infect. Dis. Poverty 6, 1–20.

Léonard, J., Dumas, N., Caussé, J.-P., Maillot, S., Giannakopoulou, N., Barre, S., Uhring, W., 2014. Lab Chip 14, 4338–4343.

Lightbody, T.O., Nightingale, P., Reddy Kolanu, V., Sapey, E., 2017. J. Diabetes Metab. 08, 1–7.

Luo, T., Zhou, T., Zhao, Y., Liu, L., Qu, J., 2018. J. Mater. Chem. B 6, 1912–1919.

Mabey, D., Peeling, R.W., Ustianowski, A., Perkins, M.D., 2004. Nat. Rev. Microbiol. 2, 231–240.

Markwalter, C.F., Davis, K.M., Wright, D.W., 2016. Anal. Biochem. 493, 30–34.

Mashamba-Thompson, T.P., Sartorius, B., Drain, P.K., 2018. BMC Health Serv. Res. 18, 1–8.

Niclass, C., Sergio, M., Charbon, E., 2006. Proc. Adv. Phot. Count. Tech. 6372, 1–12.

Obahiagbon, U., Smith, J.T., Zhu, M., Katchman, B.A., Arafa, H., Anderson, K.S., Blain Christen, J.M., 2018. Biosens. Bioelectron. 117, 153–160.

Pais, A., Banerjee, A., Klotzkin, D., Papautsky, I., 2008. Lab Chip 8, 794–800.

Pennathur, S., Fygenson, D.K., 2008. Lab Chip 8, 649–652.

Ryder, A.G., Power, S., Glynn, T.J., 2003. Proc. Opto-irel. 2002 Opt. Photonics Technol. Appl. 4876, 827–835.

Ryu, G., Huang, J., Hofmann, O., Walshe, C.A., Sze, J.Y.Y., McClean, G.D., Mosley, A., Rattle, S.J., Demello, J.C., Demello, A.J., Bradley, D.D.C., 2011. Lab Chip 11, 1664–1670.

Salthouse, C.D., Weissleder, R., Mahmood, U., 2008. IEEE Trans. Biomed. Circuits Syst. 2, 204–211.

Sharma, S., Zapatero-Rodríguez, J., Estrela, P., O'Kennedy, R., 2015. Biosensors 5, 577–601.

Vashist, S.K., 2017. Biosensors 7, 1–4.

Vilella, E., Diéguez, A., 2012. Sensors Actuators, A Phys. 186, 163–168.

Wang, Y., Yu, L., Kong, X., Sun, L., 2017. Int. J. Nanomedicine Volume 12, 4789–4803.

Watkins, N.N., Hassan, U., Damhorst, G., Ni, H., Vaid, A., Rodriguez, W., Bashir, R., 2013. Sci. Transl. Med.

Wei, L., Yan, W., Ho, D., 2017. Sensors 17, 1–3.

World Health Organization (WHO), 2018, World Malaria report 2018, WHO, Geneva.

World Health Organization(WHO), 2017, World Malaria report 2017, WHO, Geneva.

World Health Organization (WHO), 2015, Global strategy and action plan on ageing and health (2016 -2020), WHO, Geneva.